The Astrophysical Journal, 659: L169–L172, 2007 April 20

SIGNATURES OF PLANET FORMATION IN GRAVITATIONALLY UNSTABLE DISKS

Hannah Jang-Condell and Alan P. Boss
Department of Terrestrial Magnetism, Carnegie Institution of Washington, Washington, DC 20015
Received 2006 September 25; accepted 2007 March 2; published 2007 March 15

ABSTRACT

In this Letter, we calculate simulated scattered light images of a circumstellar disk in which a planet is forming by gravitational instability. The simulated images bear no correlation to the vertically integrated surface density of the disk, but rather trace the density structure in the tenuous upper layers of the disk. Although the density at high altitudes does not bear a direct relation to activity at the midplane, the very existence of structure at high altitudes along with high time variability is an indicator of gravitational instability within the disk. The timescale for variations is much shorter than the orbital period of the planet, which facilitates observation of the phenomenon. Scattered light images may not necessarily be able to tell us where exactly a planet might be forming in a disk but can still be a useful probe of active planet formation within a circumstellar disk. Although these phenomena are unlikely to be observable by current telescopes, future large telescopes, such as the Giant Magellan Telescope, may be able to detect them.

Subject headings: planetary systems: formation — planetary systems: protoplanetary disks — radiative transfer

1. INTRODUCTION

There is an ongoing theoretical debate about the dominant formation mechanism for giant planets. Two opposite extremes exist: core accretion and disk instability. In core accretion, a solid core forms first by the collisional accumulation of planetesimals and planetary embryos and then accretes a gaseous envelope from the protoplanetary disk gas (Mizuno 1980). In the disk instability mechanism, a gaseous protoplanet forms first in a gravitationally unstable, gaseous disk (Boss 1997), and then a solid core forms by the settling and coagulation of dust grains within the protoplanet. While core accretion is generally assumed to be the dominant formation mechanism for giant planets, considerable theoretical uncertainty remains about both formation mechanisms (e.g., Durisen et al. 2007). Given this murky situation, observational constraints are likely to be crucial for deciding which mechanism, if either, dominates (Boss 2006).

Millimeter-wave telescopes should be able to probe the planet-forming midplanes of optically thick disks. The Atacama Large Millimeter Array may be able to directly image gaseous protoplanets formed by disk instability or to detect the strong self-absorption of HCO^+ emission lines caused by these dense clumps of molecular gas (Narayanan et al. 2006). The latter type of detections might also be achieved by the Submillimeter Array.

Here we consider the observational appearance of light scattered by the irregular surfaces of a marginally gravitationally unstable disk that is in the process of forming gaseous protoplanets by the disk instability mechanism. The disk model studied here (from Boss 2001) is the same as the one investigated by Narayanan et al. (2006), and this work thus provides an important comparison between what can be accomplished at optical and at millimeter wavelengths in terms of constraining giant planet formation mechanisms.

Many others have studied the observable properties of young stellar objects (YSOs). This includes the spectral energy distributions of unresolved sources (e.g., Yorke et al. 1993; Boss & Yorke 1995, 1996; Wood et al. 1998, 2002; Robitaille et al. 2006) and imaging of smooth axisymmetric disk models (e.g., Whitney & Hartmann 1992, 1993; Yorke et al. 1993; Sonnhalter et al. 1995; Kessel et al. 1998; Yorke & Bodenheimer 1999; Lucas et al. 2004). In this Letter, we discuss high-resolution imaging of a disk undergoing a dynamical process. The basis for our modeling is a three-dimensional hydrodynamic simulation rather than an analytic disk model since we are interested in the perturbations that indicate activity in the disk rather than the overall emission.

2. MODEL CALCULATION

2.1. *Disk Structure*

The disk model we adopt was calculated by Boss (2001) and is described in detail in that paper. The hydrodynamics of the disk were calculated three-dimensionally in spherical coordinates, with r as the distance from the central star, θ as the angle with respect to the axis of the disk's rotation, and ϕ as the azimuthal or longitudinal angle. Pressures and temperatures were calculated on a grid with $N_r = 100$ uniformly spaced intervals in r between 4 and 20 AU and $N_\phi = 512$ uniformly spaced intervals in ϕ between 0 and 2π. In θ, $N_\theta = 23$ values were sampled, with $0° \leq \theta \leq 90°$. The system consists of a 1 $M_\odot$ central protostar, surrounded by a gaseous disk of mass 0.091 $M_\odot$ between 4 and 20 AU. From an initially smooth disk, the system was evolved several hundred years, until a gravitationally bound clump began to form. In this study, we examine snapshots of the simulation at 335, 339, and 346 yr.

2.2. *Surface*

Simulated scattered light images are generated by treating the surface of the disk as an isotropic scatterer, with half the incident flux being absorbed and the remainder scattered isotropically. The surface of the disk is defined to be where the disk becomes optically thick to stellar irradiation. That is, if we define τ_s to be the optical depth, the surface is where $\tau_s = \frac{2}{3}$. We assume the dust is well mixed with the gas, using opacities calculated by D'Alessio et al. (2001) for a grain size distribution with maximum grain size $a_{\max} = 1$ mm, power-law index of $p = 3.5$, and a dust temperature of 100 K. They calculate the Planck opacity integrated over a stellar blackbody spectrum at 4000 K as $\kappa_P^* = 11.7$ g^{-1} cm^2. The peak wavelength for this spectrum is 0.73 μm, corresponding to the R band. We treat the star as a blackbody of radius $R_* = 2.6\ R_\odot$ radiating at a temperature of $T_* = 4000$ K.

The surface is defined to be where the line-of-sight optical depth to the star is $\tau_s = \frac{2}{3}$. This is done numerically by calculating along lines of sight from the star. To avoid numerical artifacts at the inner boundary, we skip the innermost five radial

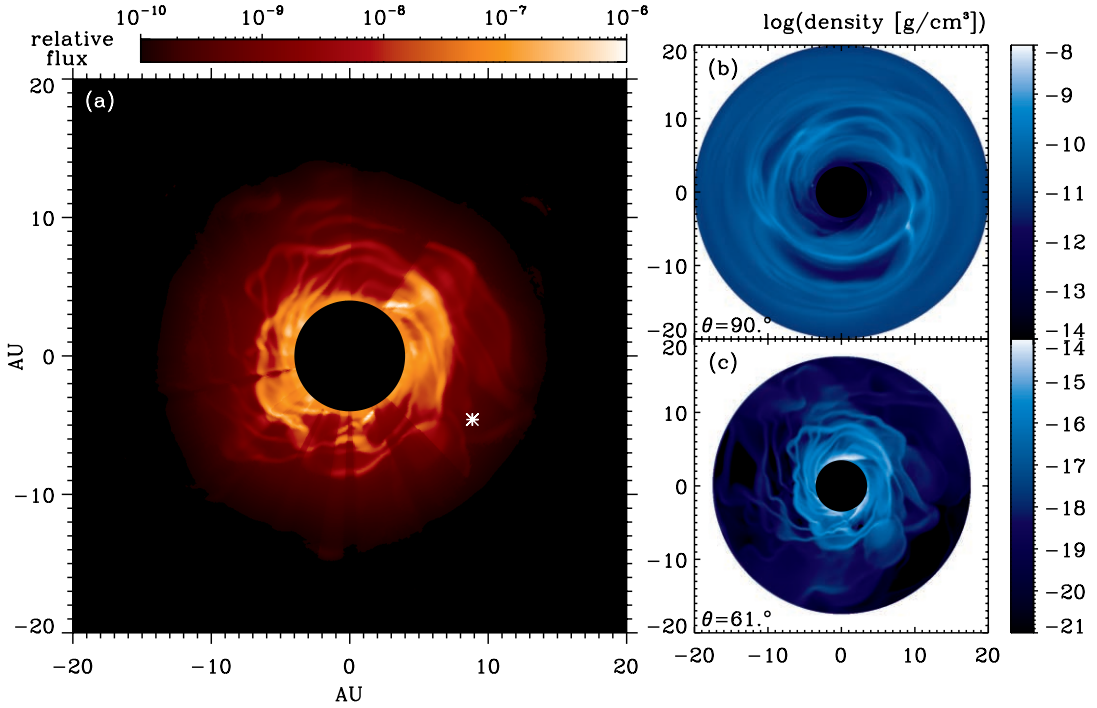

FIG. 1.—(*a*) Simulated scattered light image of a planet-forming disk, normalized to the intensity of stellar emission. As indicated by the scale bar, the intensity is displayed in the logarithm, with a maximum and minimum of 10^{-6} and 10^{-10}, respectively, of the stellar emission. The white asterisk shows the location of the forming protoplanet. The center 4 AU is outside the simulation region, so it is blacked out. (*b*) Density at the midplane of the disk. The forming planet can be clearly seen as a high-density clump. (*c*) Projected density at an opening angle of $\theta = 61°$.

grid values, so that $r_{\rm in} = r_5$. We assume that the density interior to $r_{\rm in}$ is constant [$\rho_{\rm in} = \rho(r_{\rm in})$], so

$$\tau_s(r,\ \theta,\ \phi) = \begin{cases} \kappa_{\rm P}^*\rho_{\rm in}(\theta,\ \phi)r, & r < r_{\rm in}, \\ \kappa_{\rm P}^*\ \rho_{\rm in}(\theta,\ \phi)r_{\rm in} + \displaystyle\int_{r_{\rm in}}^{r} \kappa_{\rm P}^*\rho(r',\ \theta,\ \phi)dr', & r > r_{\rm in}. \end{cases} \tag{1}$$

For a line of sight along a given direction (θ, ϕ), we calculate where the optical depth reaches $\frac{2}{3}$ and define that to be the location of the disk surface, sampling it with a resolution of $\Delta r/r < \epsilon$ or $\Delta\theta < \epsilon\mu_{\rm min}/2$, where $\mu_{\rm min} = 4R_*/3\pi r$ and $\epsilon \approx [\ln(r_{\rm max}) - \ln(r_{\rm min})]/N_r = 0.016$.

2.3. *Scattered Flux*

The flux of stellar irradiation incident on the disk at a distance r is

$$F_{\rm inc} = \sigma_B T_*^4 \left(\frac{R_*}{r}\right)^2. \tag{2}$$

The angle of incidence of stellar irradiation on the disk surface is

$$\mu = \hat{\boldsymbol{r}}\cdot\hat{\boldsymbol{n}} + \mu_{\rm min}, \tag{3}$$

where $\hat{\boldsymbol{r}}$ points from the surface to the star, and $\hat{\boldsymbol{n}}$ is normal to the surface. The finite size of the star is the reason for including the $\mu_{\rm min}$ term. To calculate the scattered flux, we assume that the surface acts like an isotropic scatterer so that half the flux is absorbed into the disk and reprocessed into thermal radiation and the other half is scattered back out isotropically. If we define $F_0 = \sigma_B T_*^4 R_*^2$ to be the flux emitted by the star, then we can express the scattered light emission relative to the stellar flux:

$$F_{\rm sca} = \frac{\mu F_0}{2r^2}. \tag{4}$$

3. RESULTS

In Figure 1*a*, we show the simulated scattered light image of the disk as calculated above, at a time of 339 yr. The flux is normalized to the stellar emission and is displayed in the logarithm as indicated by the color bar. Note that the brightest intensity is at best 10^{-6} of the stellar emission, and the minimum intensity shown is 10^{-10} of the stellar emission. The dark radial streaks seen in the simulated image are shadows of dense clumps at the inner boundary of the simulation, at 4 AU. At the distances and scales involved in the simulation, it is appropriate to treat the star as a point source, which is why the shadows diverge. The area interior to 4 AU has been blacked out to ignore numerical artifacts at the inner boundary of the simulation. The planet-forming clump is located at the position of the white asterisk. There is no apparent correlation between the position of the forming planet and structure in the scattered light image.

In Figure 1*b*, we show the density structure at the disk midplane of the simulation. The density enhancement corresponding to the position of the forming planet can be clearly seen. However, the density structure at the disk's midplane bears no resemblance to the scattered light image. In Figure 1*c*, we show the density structure of the disk at $\theta = 61°$, in projection. This is close to the height of the scattering surface of the disk. When Figures 1*a* and 1*b* are compared, it is readily apparent that the scattered light emission traces the density structure in these tenuous surface layers of the disk rather than probing the overall density structure in the

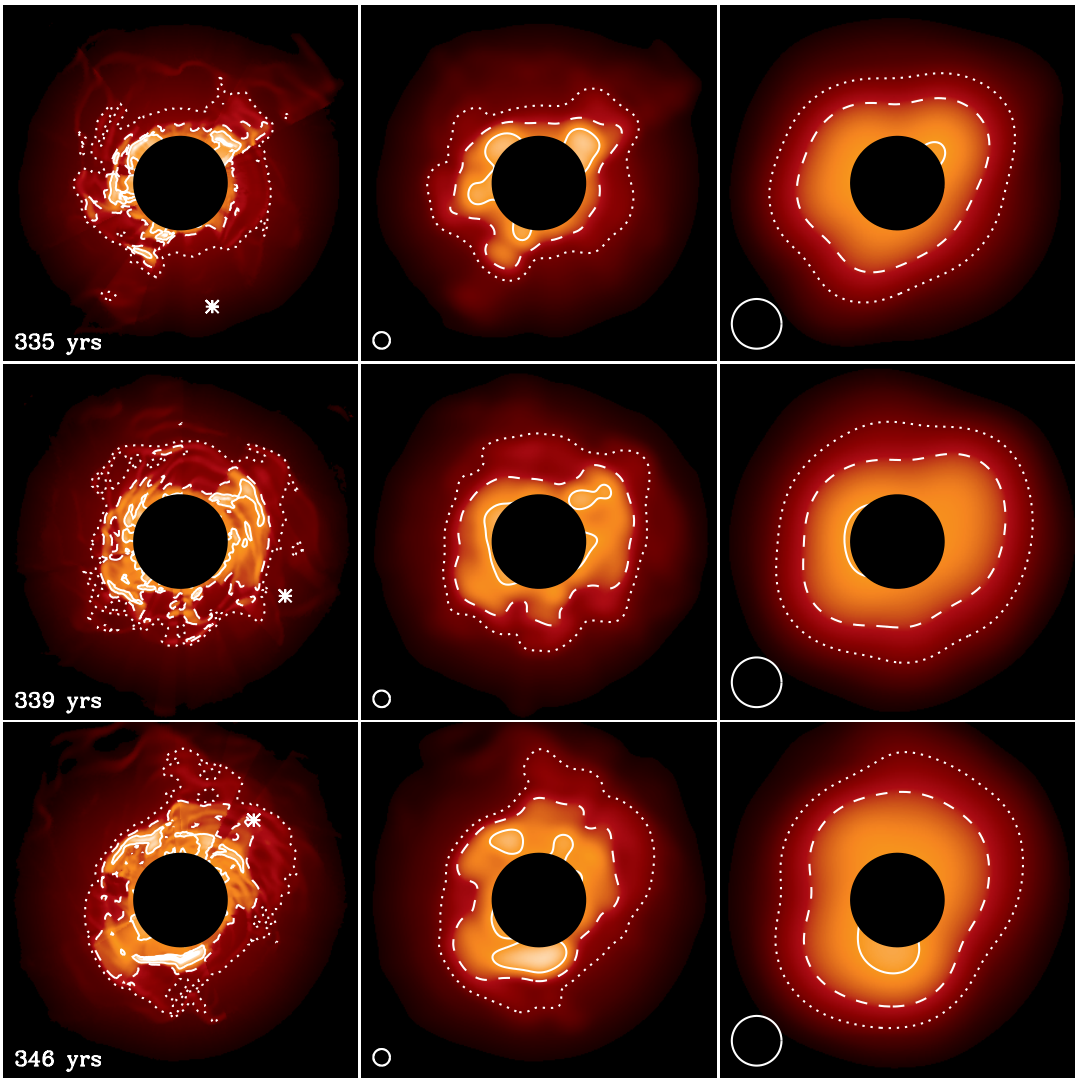

FIG. 2.—Simulated images of a disk undergoing disk instability at a simulation time of 335 (*top*), 339 (*middle*), and 346 (*bottom*) yr. The intensity scale is the same as in Fig. 1. The contours represent flux relative to stellar emission of 10^{-7} (*solid line*), 10^{-8} (*dashed line*), and 10^{-9} (*dotted line*). The left column shows the theoretical emission, with the location of the forming planet indicated by a white asterisk. The middle and right columns show the images when convolved with a PSF of 0.01″ and 0.03″, respectively. The white circles represent the sizes of these PSFs. We assume that the disk is face-on to the observer at a distance of 140 pc.

disk. The densities displayed in Figures 1*b* and 1*c* cover completely different ranges, demonstrating this fact.

The structures seen in scattered light are corrugations created in the initially smooth surfaces of the disk from the highly dynamical evolution of a marginally gravitationally unstable disk (Boss 2001). The corrugations indicate activity within the disk, even though they are not directly correlated spatially.

In Figure 2, we demonstrate the time evolution of the scattered light image. From top to bottom, we show simulated images of the disk at 335, 339, and 346 yr. For scale, the central blackout region has a diameter of 8 AU. The intensity scale is the same as in Figure 1*a* and can be inferred from the contours, which indicate flux relative to the stellar emission of 10^{-7} (*solid line*), 10^{-8} (*dashed line*), and 10^{-9} (*dotted line*). The left column shows the theoretical scattered light image, with perfect resolution, with the location of the forming planet indicated by the white asterisk. These simulated images show that the corrugations evolve on timescales of only a few years, short enough to be easily observationally detectable. Such surface irregularities are seen in other disk instability simulations as well (e.g., Boley & Durisen 2006) and can be attributed to spiral shock fronts breaking on the disk surface.

4. DISCUSSION: OBSERVABILITY

Observations of features indicative of disk instability would be a major advance for planet formation theory. An 8 m class telescope with adaptive optics would be diffraction-limited at 0.03″ at 1 μm. A 30 m class telescope such as the Giant Magellan Telescope (GMT) or the Thirty Meter Telescope, which are expected to have first light in the next decade, would have diffraction limits of less than 0.01″ at 1 μm. To illustrate what actual observations of our theoretical disks might look like, we have convolved the images in the left column of Figure 2 with Gaussian point-spread functions (PSFs) with FWHM of 0.01″ (*middle column*) and 0.03″ (*right column*). We assume that the disk is face-on to the observer at 140 pc, the approximate distance of Taurus.

A resolution of 0.01″ is just sufficient to begin resolving the corrugations in the scattered light image, while a resolution of 0.03″ reveals only some indistinct hints of structure. The Near-

Infrared Coronagraphic Imager adaptive optics coronagraph at the Gemini Observatory[1] should be diffraction-limited at 1 μm with an 8 m aperture. However, its estimated performance is a contrast ratio of 13 mag, or $10^{-5.2}$ at 1″ from the star, with decreasing performance closer to the star.

This suggests that the spatial features we have modeled may not be observable with current 8 m class telescopes and would have to wait until a 30 m class telescope such as the GMT comes online. High-contrast imaging on the GMT, which is being developed for imaging exoplanets, should be able to achieve a contrast ratio of 10^{-8} at 0.05″ at 1.65 μm (Angel et al. 2006). In comparison, the inner edge of the simulated disk at 4 AU would be at 0.06″ from the central star. The dashed contours in Figure 2 indicate a contrast ratio of 10^{-8}, so the variability in the scattered light patterns from disk instability should be observable by the GMT. Optical or infrared interferometry might also be good ways to observe disk instability. This method has already been used to detect structure in the inner 1 AU of some T Tauri disks (e.g., Akeson et al. 2005).

The temporal variations may be observable if the disk is revisited over several years. Observing this phenomenon requires finding a Class I YSO with the right orientation and without too much obscuration by an envelope. Bipolar outflows that are common to many YSOs may clear away envelope material along the poles, allowing a clear view to the inner regions of the disk that are of interest.

Since the contrast between the disk and the star is 10^{-6} at best, temporal variations in overall brightness of the unresolved source are more likely due to stellar activity than to disk activity. If the disk is resolved, then disk activity should be readily distinguished from stellar activity since the scattered light should scale with stellar brightness. Stellar activity that affects the luminosity of the star isotropically should not affect the contrast ratio between star and disk.

Anisotropic variations, such as cold or hot star spots, can be distinguished from disk activity because these variations will have the same period as the rotation period of the star, which is on the order of days for typical young stars. For example, HH 30 is an edge-on disk system whose periodic fluctuations in brightness are caused by illumination from a hot spot on the star sweeping across the surface of the disk as the star rotates, similar to a lighthouse (Wood et al. 1998; Wood & Whitney 1998; Cotera et al. 2001). This variability occurs on timescales of days and is periodic. In contrast, the features we have modeled vary over years and are irregular. By monitoring an object over a series of several nights, short-term effects can be filtered out and the year-to-year variations can be studied to determine if activity characteristic of disk instability is occurring.

In contrast to the variability characteristic of disk instability, planet formation by core accretion should be more quiescent, resulting in a distinct shadow at the position of the forming planet core (Jang-Condell 2005a, 2005b). The mechanisms are also separated in pre–main-sequence evolutionary epochs: disk instability is expected to occur during the Class I phase of star/planet formation, where there is substantial disk and envelope material infalling toward the star. Core formation has a much longer expected timescale, so those signatures are detectable during the Class II phase, after the envelope has cleared but the disk still remains.

5. CONCLUSIONS

Since scattered light images of optically thick disks give information about the tenuous upper layers of the disk rather than the overall large-scale structure, one should be cautious when trying to infer disk structure from scattered light images. For example, the outer disk of AB Aurigae (Fukagawa et al. 2004) extends out to hundreds of AU, and over that path length, even a small amount of material can easily block stellar illumination. This effect should be considered before drawing strong conclusions about the underlying disk structure.

Although scattered light emission is not directly correlated to the planet forming in the disk, the presence of structure in the scattered light emission coupled with high time variability can be an indicator of planet-forming activity. We can at least identify disks where planets are forming even if we cannot say exactly where in the disk it is taking place. The GMT might well be able to detect these rapid variations in scattered light on spatial scales of interest (~5–10 AU) for giant planet formation and thus shed light on the processes occurring deep inside optically thick protoplanetary disks.

Emission from the disk itself at longer wavelengths should be a better probe of the overall disk structure both because the optical depth is smaller at longer wavelengths and because direct emission from the disk has better contrast with respect to the star than scattered light. Observations of gravitationally unstable disks in the millimeter and submillimeter, such as those predicted by Narayanan et al. (2006), will be a useful complement to those predicted in this Letter.

We thank John Chambers for helpful discussions in the preparation of this Letter and our anonymous referee for helpful comments that greatly improved it. The authors acknowledge support by the NASA Astrobiology Institute under Cooperative Agreement NNA04CC09A.

[1] See http://www.gemini.edu/sciops/instruments/nici/niciIndex.html.

REFERENCES

Akeson, R. L., et al. 2005, ApJ, 622, 440
Angel, R., Codona, J. L., Hinz, P., & Close, L. 2006, Proc. SPIE, 6267, 62672A
Boley, A. C., & Durisen, R. H. 2006, ApJ, 641, 534
Boss, A. P. 1997, Science, 276, 1836
———. 2001, ApJ, 563, 367
———. 2006, in Planet Formation 2004: Observations, Experiments, and Theory, ed. H. Klahr & W. Brandner (Cambridge: Cambridge Univ. Press), 192
Boss, A. P., & Yorke, H. W. 1995, ApJ, 439, L55
———. 1996, ApJ, 469, 366
Cotera, A. S., et al. 2001, ApJ, 556, 958
D'Alessio, P., Calvet, N., & Hartmann, L. 2001, ApJ, 553, 321
Durisen, R., Boss, A., Mayer, L., Nelson, A., Rice, K., & Quinn, T. 2007, in Protostars and Planets V, ed. B. Reipurth, D. Jewitt, & K. Keil (Tucson: Univ. Arizona Press), 607
Fukagawa, M., et al. 2004, ApJ, 605, L53
Jang-Condell, H. 2005a, BAAS, 37, 1426
Jang-Condell, H. 2005b, Poster Abstract at Protostars and Planets V (Hilton Waikoloa Village, HI), 8576
Kessel, O., Yorke, H. W., & Richling, S. 1998, A&A, 337, 832
Lucas, P. W., et al. 2004, MNRAS, 352, 1347
Mizuno, H. 1980, Prog. Theor. Phys., 64, 544
Narayanan, D., Kulesa, C. A., Boss, A., & Walker, C. K. 2006, ApJ, 647, 1426
Robitaille, T. P., Whitney, B. A., Indebetouw, R., Wood, K., & Denzmore, P. 2006, ApJS, 167, 256
Sonnhalter, C., Preibisch, T., & Yorke, H. W. 1995, A&A, 299, 545
Whitney, B. A., & Hartmann, L. 1992, ApJ, 395, 529
———. 1993, ApJ, 402, 605
Wood, K., Kenyon, S. J., Whitney, B., & Turnbull, M. 1998, ApJ, 497, 404
Wood, K., Lada, C. J., Bjorkman, J. E., Kenyon, S. J., Whitney, B., & Wolff, M. J. 2002, ApJ, 567, 1183
Wood, K., & Whitney, B. 1998, ApJ, 506, L43
Yorke, H. W., & Bodenheimer, P. 1999, ApJ, 525, 330
Yorke, H. W., Bodenheimer, P., & Laughlin, G. 1993, ApJ, 411, 274